

The effects of baryons on the halo mass function

Weiguang Cui^{1*}, Stefano Borgani^{1,2,3}, Klaus Dolag^{4,5}, Giuseppe Murante⁶,
Luca Tornatore¹

¹ *Astronomy Unit, Department of Physics, University of Trieste, via Tiepolo 11, I-34131 Trieste, Italy*

² *INAF, Osservatorio Astronomico di Trieste, via Tiepolo 11, I-34131 Trieste, Italy*

³ *INFN – National Institute for Nuclear Physics, Trieste, Italy*

⁴ *Universitätssternwarte München, München, Germany*

⁵ *Max-Planck-Institut für Astrophysik, Garching, Germany*

⁶ *INAF, Osservatorio Astronomico di Torino, Str. Osservatorio 25, I-10025, Pino Torinese, Torino, Italy*

5 April 2012

ABSTRACT

We present an analysis of the effects of baryon physics on the halo mass function. The analysis is based on simulations of a cosmological volume having a comoving size of $410 h^{-1}$ Mpc, which have been carried out with the Tree-PM/SPH GADGET-3 code, for a WMAP-7 Λ CDM cosmological model. Besides a Dark Matter (DM) only simulation, we also carry out two hydrodynamical simulations: the first one includes non-radiative physics, with gas heated only by gravitational processes; the second one includes radiative cooling, star formation and kinetic feedback in the form of galactic ejecta triggered by supernova explosions. All simulations follow the evolution of two populations of 1024^3 particles each, with mass ratio such to reproduce the assumed baryon density parameter, with the population of lighter particles assumed to be collisional in the hydrodynamical runs. We identified halos using a spherical overdensity algorithm and their masses are computed at three different overdensities (with respect to the critical one), $\Delta_c = 200, 500$ and 1500 .

We find the fractional difference between halo masses in the hydrodynamical and in the DM simulations to be almost constant, at least for halos more massive than $\log(M_{\Delta_c}/h^{-1} M_\odot) \geq 13.5$. In this range, mass increase in the hydrodynamical simulations is of about 4–5 per cent at $\Delta_c = 500$ and $\sim 1 - 2$ per cent at $\Delta_c = 200$. Quite interestingly, these differences are nearly the same for both radiative and non-radiative simulations. Mass variations depends on halo mass and physics included for higher overdensity, $\Delta_c = 1500$, and smaller masses. Such variations of halo masses induce corresponding variations of the halo mass function (HMF). At $z = 0$, the HMFs for GH and CSF simulations are close to the DM one, with differences of $\lesssim 3$ per cent at $\Delta_c = 200$, and $\simeq 7$ per cent at $\Delta_c = 500$, with $\sim 10 - 20$ per cent differences reached at $\Delta_c = 1500$. At this higher overdensity, the increase of the HMF for the radiative case is larger by about a factor 2 with respect to the non-radiative case. Assuming a constant mass shift to rescale the HMF from the hydrodynamic to the DM simulations, brings the HMF difference with respect to the DM case to be consistent with zero, with a scatter of $\lesssim 3$ per cent at $\Delta_c = 500$ and $\lesssim 2$ per cent at $\Delta_c = 200$.

Our results have interesting implications to assess uncertainties in the mass function calibration associated to the uncertain baryon physics, in view of cosmological applications of future large surveys of galaxy clusters.

Key words: clusters: cosmology: theory – dark matter – galaxies: formation – halos – methods: numerical

1 INTRODUCTION

An accurate calibration of the halo mass function is at the hearth of a range of cosmic structure formation studies, from

* wgcai@oats.inaf.it

the study of galaxy formation through semi-analytical models (e.g. Baugh 2006), to the cosmological application of galaxy clusters (Allen et al. 2011). Under the standard hierarchical Λ CDM model, halos are formed from initial density peaks through gravitational instability. The halo mass function (HMF hereafter) is directly connected to the primordial density field. Since the abundance of density peaks over a given mass scale M only depends on the r.m.s. value σ_M of the linear fluctuation field at that mass scale, the abundance of halos is expected to be universal once expressed as a function of σ_M , as assumed by the Press-Schechter approach based on the spherical collapse model (Press & Schechter 1974) and in the ellipsoidal collapse extension by Sheth & Tormen (1999).

Through the years, N-body simulations of large cosmological volumes have been used to calibrate fitting functions for a universal HMF (e.g. Jenkins et al. 2001; Warren et al. 2006; Springel et al. 2005; Lukić et al. 2007). Thanks to the progressive increase in the covered dynamic range of halo masses, simulation results have been shown to predict subtle but sizable deviations from universality of the mass function. For instance Reed et al. (2003) found that the universal mass function by Sheth & Tormen (1999) over-predicts the number of most massive halos found at $z > 10$. This result was confirmed by the subsequent analysis by Reed et al. (2007), who pointed out that an even better fit for the mass function can be obtained if it is allowed to depend not only on the linear r.m.s. overdensity, but also on the local slope of the linear power spectrum at the relevant mass scale. Using the spherical over-density (SO) algorithm to measure cluster masses, Tinker et al. (2008) combined different simulations to calibrate the HMF, with masses measured at different overdensities. They found significant deviations from non-universality, with a monotonic decrease of halo abundance with increasing redshift, and provided fitting functions to such deviation. Besides confirming the non-universal behaviour of the high end of the HMF, Crocce et al. (2010); Tinker et al. (2008) also pointed out that using more accurate second-order Lagrangian perturbation theory to set initial conditions could be relevant for an accurate HMF calibration. Bhattacharya et al. (2011) analyzed the HMF for an extended suite of simulations also including quintessence models with $w \neq -1$ for the Dark Energy equation of state, and confirmed violation of universality at the ~ 10 per cent level for the range of masses and redshift covered by their simulations.

At least in principle, calibrating the mass function of DM halos with great accuracy is just a technical problem to be tackled by extending the dynamic range of simulations and the parameter space of considered cosmological models. However, the back-reaction effects of baryons on dark matter halos are known to impact on density profiles and, therefore, on their mass. In turn, these back-reaction effects are expected to depend on the detail of the physical processes, such as radiative cooling, star formation and energy feedback from astrophysical sources, which determine the distribution of baryons within DM halos. Tinker et al. (2008) included a non-radiative hydrodynamical simulation of a large cosmological volume within the large set of simulations that they analyzed, without however discussing in detail the effect of baryons on the HMF. Rudd et al. (2008) compared the HMF computed for a DM-only simulation with those ob-

tained from the corresponding hydro-dynamical simulations, carried out with an Adaptive Mesh Refinement (AMR) code both with non-radiative physics and including the effect of gas cooling and star formation. After computing masses at the viral radius, they found that the HMF for non-radiative simulation is very close to the DM-only one, at least in the mass range numerically resolved by both simulations. On the other hand, the radiative simulation was found to produce a $\simeq 10$ per cent higher mass function, as a consequence of the higher concentration halo concentration resulting from adiabatic contraction (e.g. Gnedin et al. 2004). A significant increase of halo concentration from adiabatic contraction is a well known consequence of (over)efficient gas cooling (e.g. Pedrosa et al. 2009; Tissera et al. 2010; Duffy et al. 2010). In line with this result on halo concentration, also the total matter power spectrum in radiative hydrodynamic simulations has been shown to have a higher amplitude than for DM-only N-body simulations, small non-linear scales $k > 1 h Mpc^{-1}$ (Rudd et al. 2008; Jing et al. 2006; van Daalen et al. 2011; Casarini et al. 2011, ; Casarini et al., in preparation). However, also the simple case of non-radiative hydrodynamics has been suggested to increase halo concentration, as a consequence of a redistribution of energy between baryons and DM during halo collapse (Rasia et al. 2004; Lin et al. 2006). An increase of halo concentration turns into an increase of halo masses, hence increasing the halo mass function. Zentner et al. (2008) suggested that the main effects of baryons can be translated into a simple change of halo concentrations, thereby resulting in a uniform relative shift of halo masses. Stanek et al. (2009) compared the cluster masses and mass functions for a set of simulations including only DM, non radiative hydrodynamics, as well as radiative runs with and without pre-heating. They reported for the pre-heated run an average decrease of halo mass M_{500}^1 by 15 percent with respect to the non-radiative case, and 16 percent halo mass enhancement for simulation with cooling and star formation (CSF) with respect to the DM simulation. These mass variations turn into differences of the HMF of up to ~ 30 percent. Stanek et al. (2009) based their analysis on two different sets of simulations, based on SPH and AMR codes, also using slightly different choices for the cosmological parameters. Furthermore, results for their CSF case were based only on re-simulations of the 13 most massive halos identified in the original simulation volume.

In order to improve with respect to the current understanding of baryon effects on the HMF, we present in this paper the analysis of three cosmological simulations based on DM only, non-radiative hydrodynamics and cooling, star formation and supernova (SN) feedback. These simulations are carried out starting from the same initial conditions and using the same Tree-PM/SPH code GADGET-3 Springel (2005a). Resolution and box-size of our simulations are adequate to cover the halo mass distribution over the range $\log(M_{200}/h^{-1} M_\odot) \simeq (12.5 - 15)$ at $z = 0$. Due to the inclusion of hydrodynamics, the dynamic range covered by our simulations is in general narrower than that accessible by

¹ In the following, we will use the convention R_{Δ_c} to indicate the halo radius encompassing an average overdensity of Δ_c times the critical cosmic density $\rho_{cr}(z)$. Accordingly, M_{Δ_c} is the halo mass contained within R_{Δ_c} .

N-body simulations used over the last few years for precision calibrations of the HMF. For this reason, the aim of this paper is not that of providing one more of such calibrations, rather our goal is to assess in detail the impact of baryons on the HMF.

This paper is organized as follows. In Section 2, we describe the simulations. Section 3 is devoted to the presentation of the analysis method and results. After describing the halo identification method based on spherical overdensity, we present the results of our analysis in terms of mass variation of halos and resulting effect on the HMF. Finally, we discuss our results and present the main conclusions in Section 4.

2 THE SIMULATIONS

We carry out simulations of a flat Λ CDM cosmology with $\Omega_m = 0.24$ for the matter density parameter, $\Omega_b = 0.0413$ for the baryon contribution, $\sigma_8 = 0.8$ for the power spectrum normalization, $n_s = 0.96$ for the primordial spectral index, and $h = 0.73$ for the Hubble parameter in units of $100 \text{ km s}^{-1} \text{ Mpc}^{-1}$. Initial conditions have been generated at $z = 49$ using the Zeldovich Approximation for a periodic cosmological box with comoving size $L = 410 h^{-1} \text{ Mpc}$. Initial density and velocity fields are sampled by displacing, at redshift $z = 41$, the positions of two sets of 1024^3 particles each, according to the Zeldovich approximation, from unperturbed positions located onto two regular grids which are shifted by half grid size with respect to each other. Masses of the particles belonging to the two sets have ratio such that to reproduce the cosmic baryon fraction, with $m_1 \simeq 3.54 \times 10^9 h^{-1} \text{ M}_\odot$ and $m_2 \simeq 7.36 \times 10^8 h^{-1} \text{ M}_\odot$. In the DM-only simulation both particle species are treated as collisionless, while in the hydro-dynamical simulations m_2 provides the mass of gas particles. We emphasize that this prescription to set initial conditions for the DM simulation ensures that it starts exactly from the same sampling of density and velocity field as its hydro-dynamical counterpart. Convergence of the mass function against changing initial redshift and effect of using second-order Lagrangian Perturbation Theory (2LPT) have been discussed by Tinker et al. (2008) and Crocce et al. (2010). Although small but sizeable effects have been detected in the high-end of the mass function, the general result is that the effect of 2LPT is rather small for initial redshift and resolution relevant for our simulations. Furthermore, since our analysis is focussed on the relative effect induced by the presence of baryons, we expect the main conclusions not to be affected by increasing the accuracy in the computation of displacements in the generation of initial conditions.

Simulations are carried out using the TreePM-SPH code GADGET-3, an improved version of the GADGET-2 code (Springel 2005b). In GADGET-3 domain decomposition is performed by allowing disjointed segments of the Peano-Hilbert curve to be assigned to the same computing unit, thus turning into a significant improvement of the workload balance when run over a large number of processors. Gravitational forces have been computed using a Plummer-equivalent softening which is fixed to $\epsilon_{Pl} = 7.5 h^{-1}$ physical kpc from $z = 0$ to $z = 2$, and fixed in comoving units at higher redshift.

Besides a DM-only simulation (DM hereafter), we also carried out two hydrodynamical simulations. A non-radiative simulation only including gravitational heating of the gas (GH hereafter) used 64 neighbours for the computation of hydrodynamic forces, with the width of the B-spline smoothing kernel allowed to reach a minimum value equal to half of the gravitational softening. A second hydrodynamical simulation has been carried out by including the effect of cooling and star formation (CSF hereafter). In this simulation radiative cooling is computed for non-vanishing metallicity according to Sutherland & Dopita (1993), also including heating/cooling from a spatially uniform and evolving UV background. Gas particles above a given threshold density are treated as multi-phase, so as to provide a sub-resolution description of the interstellar medium, according to the model described by Springel & Hernquist (2003). In each multi-phase gas particle, a cold and a hot-phase coexist in pressure equilibrium, with the cold phase providing the reservoir of star formation. Conversion of collisional gas particles into collisionless star particles proceeds in a stochastic way, with gas particles spawning a maximum of two generations of star particles. The CSF simulation also includes a description of metal production from chemical enrichment contributed by SN-II, SN-Ia and AGB stars, as described by (Tornatore et al. 2007). Kinetic feedback is implemented by mimicking galactic ejecta powered by SN explosions. In these runs, galactic winds have a mass upload proportional to the local star-formation rate. We use $v_w = 500 \text{ km s}^{-1}$ for the wind velocity, which corresponds to assuming about unity efficiency for the conversion of energy released by SN-II into kinetic energy for a Salpeter IMF. The feedback model included in the CSF simulation is known not to be able to regulate overcooling, especially in large cluster-sized halos (e.g. Borgani et al. 2004). To show this, we implement a consistent comparison in Figure 1, between observational results on the mass fraction in stars within R_{500} (from Gonzalez et al. 2007; see also Gonzalez et al. 2007; Lagana et al. 2011) and results obtained from the analysis of the clusters and groups identified in the CSF simulation. Quite apparently, simulations predict a decline of the stellar mass fraction as a function of cluster mass which is much milder than the observed one. As a result, massive systems in simulations are predicted to have an exceedingly high mass fraction in stars. Therefore, while none of the two hydrodynamical simulations provides a fully correct description of the evolution of baryons within DM halos, considering both the GH and the CSF runs one should provide a useful indication of the impact of current uncertainties in the description of baryon physics.

3 RESULTS

3.1 Halo identification

The two most common methods for halo identifications simulations are the one based on the Friend-of-Friend (FoF) algorithm (e.g. Davis et al. 1985) and that based on the spherical overdensity (SO) algorithm (Lacey & Cole 1994). The FoF halo finder has only one parameter, b , which defines the linking length as bl where $l = n^{-1/3}$ is the mean inter-particle separation, with n the mean particle number

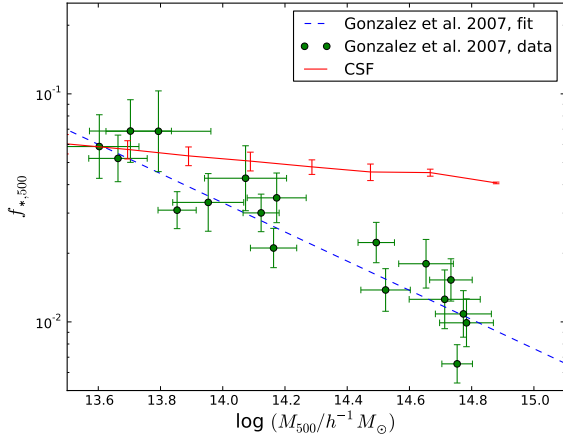


Figure 1. Comparison between observational results and simulations on f_* , defined as the stellar mass fraction within R_{500} , for groups and clusters of galaxies. Circles with errorbars are the observational results for the clusters and groups analysed by Gonzalez et al. (2007), with the dashed line showing the best-fit linear regression to these data points. The continuous line shows the results for the halos identified in the CSF simulations. Errorbars in this case refer to the r.m.s. scatter within each interval in M_{500} .

density. In the SO algorithm there is also only one free parameter, namely the mean density $\Delta_c \rho_{crit}$ contained within the sphere within which halo mass is computed, with ρ_{crit} being the critical cosmic density. Each of the two halo finders has its own advantages and shortcomings (see more details in Jenkins et al. 2001; White 2001; Tinker et al. 2008, etc), and the difference of halo mass and HMF defined by the two methods have been discussed in several analysis, (e.g. White 2002; Reed et al. 2003, 2007; Cohn & White 2008; Tinker et al. 2008; More et al. 2011).

In our analysis we apply the SO method, with masses measured at four different overdensities corresponding to $\Delta_c = 200, 500$ and 1500 , thus ranging from the overdensity which characterize the whole virialized region of halos up to the typical overdensity which is accessible by Chandra and XMM–Newton X–ray observations. Our halo identification proceeds in two steps. In the first step we run a FoF algorithm with linking length $b = 0.16$ over the distribution of DM particles (in the DM-only simulation the FoF is run over the distribution of more massive particles). Then, we identify in each FoF group the DM particle which corresponds to the minimum of the potential. The position of this particle is taken to be the center of the cluster from where to grow spheres whose radius is increased until the mean density within it reaches the required overdensity Δ_c . The mass M_{Δ_c} within this spherical region of radius R_{Δ_c} is

$$M_{\Delta_c} = \frac{4}{3} \pi R_{\Delta_c}^3 \Delta_c \rho_{crit}(z). \quad (1)$$

Since each halo is firstly identified starting from a FoF algorithm, it inherits some FoF disadvantages. A well known potential problem with FoF is that there are situations in which two halos are connected through a bridge of particles. Since this halo is counted only once, this could affect the number of SO halo number and the resulting mass function.

As discussed by (Reed et al. 2007), this effect becomes more important at high redshift and for poorly resolved low-mass halos. Since we restrict our analysis to halos having a minimum mass of $10^{13} h^{-1} M_{\odot}$, thus being resolved by at least 10^4 particles) and redshift $z \leq 1$, and we use a linking length smaller than the usually adopted value $b = 0.2$, we expect the bias induced by using FoF parent groups should be mitigated. Since the FoF grouping is carried out using DM particles as primary particles, we expect halo bridging to affect in the same way the N-body and the different hydrodynamical simulations. Therefore, our main conclusions on the relative effect of baryons on the mass function should be left unchanged by the effect of using FoF groups as the starting point of the SO identification. Finally, since the groups identified by FoF algorithm have by definition no overlapping, we do not include in our identification of SO halos any restriction to prevent such overlapping (see Tinker et al. 2008 for a discussion on halo overlapping).

3.2 Effect on halo mass and density profile

We first focus on the impact that baryons have on the mass of individual halos. To this purpose, we show in Figure 2 the distribution of the differences between halos identified in the two hydrodynamical simulations and in the DM simulation, at different overdensities. Results in this figure are shown for all the halos that in the DM simulation have $M_{\Delta} \geq 10^{14} h^{-1} M_{\odot}$. To compare halo masses, one has to identify a halo selected in the DM simulation with its counterpart in each one of the hydrodynamical simulations. The easiest way to perform this identification is to look for the halos having the closest coordinates. While this procedure provides a reliable identification of corresponding halos in two different simulations for the most massive systems, it turns out not to be accurate for poorer systems. In fact, besides affecting the mass of halos, the presence of baryons also slightly alter the overall dynamics and, therefore, the exact halo positions. In order to overcome this difficulty we decided to follow a different procedure to find in each of the hydrodynamical simulations the halos corresponding to those identified in the DM run. For each halo in the DM simulation we identify the Lagrangian region from where particles following within its virial radius by $z = 0$ come from. We then look in each of the GH and CSF simulations for a halo that contains at least 60 per cent of the particles coming from the same Lagrangian region. We verified that the final results do not change significantly if we use instead a more restrictive requirement to find instead 80 per cent of the particles from the same Lagrangian region.

From Fig. 2, we see that significant mass differences, of up to 20 per cent, are found for $\Delta_c = 1500$, with the distribution of such differences becoming narrower at $\Delta_c = 200$. Correspondingly, the mean value of the halo mass increase induced by the presence of baryons decreases from $\simeq 6$ –7 per cent at $\Delta_c = 1500$ to $\simeq 3$ –4 per cent at $\Delta_c = 500$, while being $\lesssim 1$ per cent at $\Delta_c = 200$. Furthermore, any differences between the two hydrodynamic runs is much smaller than the difference that each of them has with respect to the DM run. This result is in line with the weak sensitivity of the mass function on the details of the baryon physics, as shown in Fig. 5. Even at the highest considered overdensity, $\Delta_c = 1500$, there is a small number of halos whose mass in

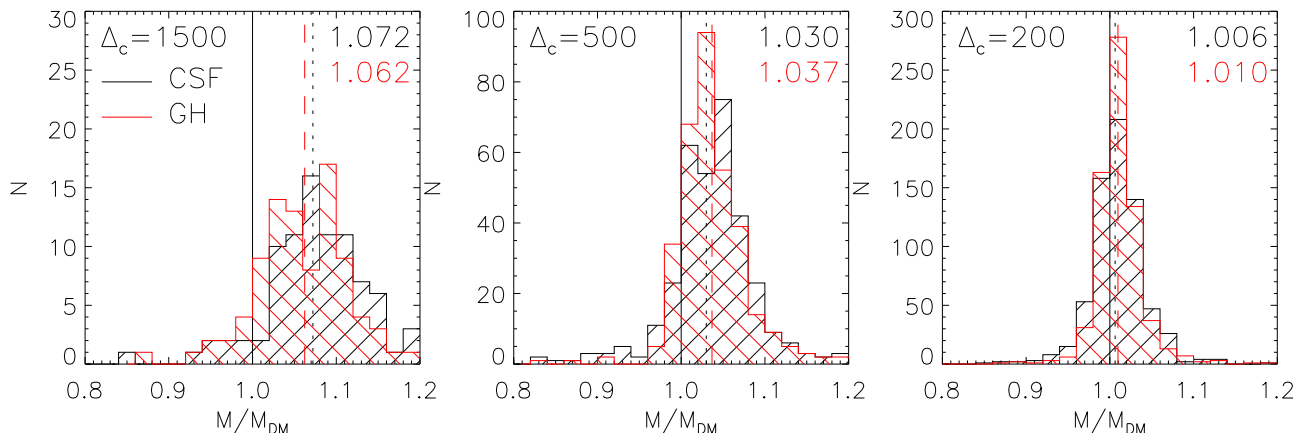


Figure 2. The distribution of the mass ratios between the halos identified in each of the two hydrodynamical simulations to the corresponding halos in the DM simulation. The three panels from left to right show the results at $\Delta_c = 1500, 500, 200$. Red and black continuous histograms show the results for M_{GH}/M_{DM} and M_{CSF}/M_{DM} , respectively. In each panel, results are shown only for halos with $M_{\Delta_c} \geq 10^{14} h^{-1} M_\odot$. The solid vertical lines correspond to no mass variation, while the dashed and dotted vertical lines show the mean values (which is shown on the right-top of each panel) of M_{GH}/M_{DM} and M_{CSF}/M_{DM} , respectively.

the hydrodynamical runs is smaller than in the DM run. The reason for this is the different timing of merging of substructures in the different simulations. This occasionally causes some of these substructures to be found outside R_{1500} while located within this radius in the DM simulation.

In order to quantify a possible mass dependence of this halo mass difference, we show in Figure 3 the mean value of such a difference for each mass bin where the mass function is computed. Throughout our analysis, we use a fixed mass bin with width $\Delta \log M = 0.2$. With such a narrow bin, the mass function suffers for large sampling effect in the high-mass end, due to the exponential dearth of the massive halo population. To overcome such sampling effect, we merge mass bins containing less than 10 objects into the adjacent lower mass bin. Each mass bin is then weighted proportionally to the number of clusters it contains.

The increase of halo masses in both the GH and CSF simulations is to good approximation independent of halo mass, at least for $\log(M/h^{-1} M_\odot) \gtrsim 13.5$, at overdensities $\Delta_c = 200$ and 500. Again, this shift in mass turns out to be similar in the two hydrodynamical runs. It amounts to about 1–2 per cent at $\Delta_c = 200$ and $\simeq 4$ per cent at $\Delta_c = 500$, in line with the results shown in Fig. 2. The increasing star formation efficiency in lower mass halos makes the mass increase in the CSF simulation to be larger than for the GH case. This difference between GH and CSF halo masses further increases for $\Delta_c = 1500$. At this overdensity we can not define a mass range over which the increase of halo masses due to baryons is nearly constant and independent of gas physics.

To better understand the origin of the mass difference between halos identified in different simulations, we further show in Figure 4 the radial profile of the mean total density for halos identified in the three simulations. The four panels correspond to different mass ranges. Since density is normalized to ρ_{200} , i.e. the mean density within R_{200} , the profiles reach the unity value for $R/R_{200} = 1$. As for the halos identified in the GH simulation (red dot-dashed curves), their profiles have small but sizable differences with

respect to the DM case (solid black curves). At intermediate radii, $0.1 \lesssim R/R_{200} \lesssim 1$ the GH profiles lie above those of the DM simulation. This result, which holds independent of the halo mass, is consistent with that found by Rasia et al. (2004) in their comparison of halo profiles from DM-only and non-radiative hydrodynamical simulations. These authors argued that the more concentrated density profiles in non-radiative simulations, with respect to DM-only simulations, is the result of energy redistribution between the DM and the baryonic component during halo collapse (see also Lin et al. 2006). We postpone to a forthcoming paper a detailed comparison between concentrations for halos identified in DM and hydrodynamic simulations (Rasia et al. in preparation). It is only at small radii, $R \lesssim 0.08 R_{200}$, that gas pressure support makes the total density profiles in the GH simulation slightly flattening with respect to the DM simulation.

As for the radiative CSF simulation (blue dashed curves), the sinking of cooled baryons, converted into stars, in the central halo regions causes the already known effect of adiabatic contraction, with the resulting steepening of the density profiles in these regions. A comparison of the resulting profiles for the different mass ranges indicates that this effect is more pronounced for halos of smaller mass, consistent with the expectation that cooling is in fact more efficient in lower mass halos, due to their higher concentration. The effect of gas cooling is rather pronounced for $R \lesssim 0.2 R_{200}$. We note that the vertical purple line in Figure 4 mark the mean value of R_{1500} for halos of the DM simulation. The corresponding value of R_{1500} for the CSF simulation is in fact slight larger than in the DM case. This difference explains why halo masses in the CSF simulation are only slightly larger than in the GH simulation already at R_{1500} .

3.3 Effect on the Halo Mass Function

In order to compute the mass function, we group SO halos within mass bins having fixed width $\Delta \log M = 0.2$. Then,

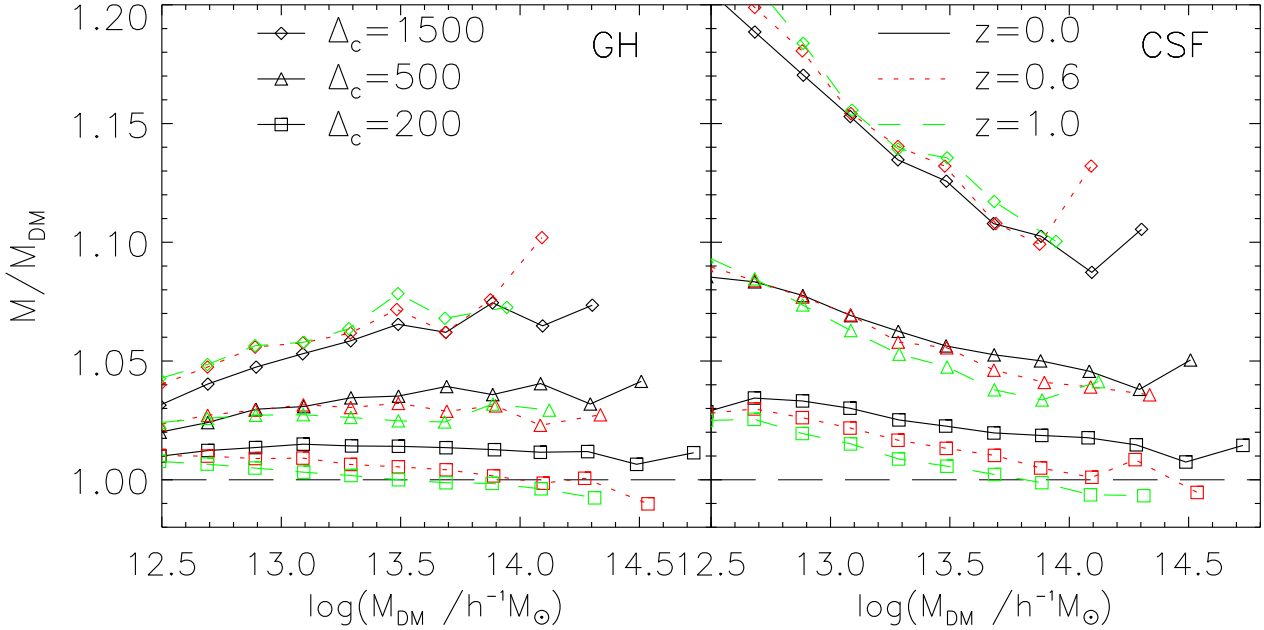


Figure 3. The ratio between masses of halos identified in the hydrodynamical simulations and the corresponding halos from the DM simulation, as a function of halo mass in the DM run, M_{DM} . Left and right panels show the results for the GH and CSF run, respectively. In each panel different line styles, associated with different colors, corresponds to different redshifts. Different symbols indicate instead different Δ_c . For reference, the horizontal light long-dashed line correspond to no mass variation.

the mass assigned to each bin is computed as the mean over all the halos belonging to that mass bin. Whatever procedure one adopts to choose the mass to be assigned to a given bin, it is clear that the binning procedure introduce an uncertainty in the resulting mass function. As discussed by Lukić et al. (2007), this uncertainty is negligible as long as the bin width does not exceed $\Delta \log M = 0.5$.

We show in Figure 5 the HMF for our three simulations, computed for $\Delta_c = 200, 500, 1500$ (from upper to lower groups of curves). To better emphasize the mass variation induced by the presence of baryons, we show in the lower panel the difference in the number of clusters within each mass bin, between each of the two hydrodynamical simulations and DM simulation. Due to the specific treatment of the last bin, its width can be different for different simulations. Therefore, when we compare the number of objects in such last bins, we rescale the cluster counts within each of them by scaling it to the bin width in units of $\Delta \log M = 0.2$.

In general, we find that the presence of baryons leads to an increase of the HMF by an amount increasing as we move to more internal regions at higher Δ_c . In general, this variation is nearly independent of mass, except possibly in the high mass end, beyond $\log(M/h^{-1} M_\odot) \simeq 14.5$. This is the regime where exponential tail takes place. Given the limited box size, the resulting limited statistics of massive halos does not allow us to draw robust conclusions for such high masses, especially when considering $\Delta_c = 500$ and above. For the GH non-radiative simulation the HMF increase is negligible at $\Delta_c = 200$, and amounts to $\lesssim 3$ per cent at the largest sampled masses. This difference increases to $\lesssim 8$ per cent as we move to $\Delta_c = 500$, at least up to $\log(M/h^{-1} M_\odot) \simeq 14.5$. We note that at such overdensities the effect of introducing baryons produce a variation of the HMF with respect to the

DM simulation which is larger than the difference between the GH and the CSF run. This indicates that, while it is important to account for the presence of baryons in the HMF calibration for $\Delta_c \lesssim 500$, the details of the physical processes regulating their evolution has a minor impact. At a higher overdensity $\Delta_c = 1500$, the effect of radiative physics is of increasing the HMF by about 20 per cent for CSF run and around 10 per cent for GH run. This result is in line with the expectation that a more concentrated density profile in the presence of gas cooling (Gnedin et al. 2004; Pedrosa et al. 2009; Tissera et al. 2010; Duffy et al. 2010).

In general, our results for an increase of the HMF for the GH simulation is in line with previous findings, also based on non-radiative simulations, for an increase of halo concentration induced by the presence of gas (Rasia et al. 2004; Jing et al. 2006; Lin et al. 2006; Rudd et al. 2008). The effect of the physics of baryons becomes more important at $\Delta_c = 1500$. In their analysis of the cumulative mass function Rudd et al. (2008) found that the presence of non-radiative gas induces a negligible HMF variation for masses estimated at the virial radius, corresponding to $\Delta_c \simeq 100$ for their simulated cosmology. While this result is in agreement with our, Rudd et al. (2008) find that the HMF increases by about 10 per cent when radiative cooling and star formation are included. One possible reason for the different effect of radiative physics in our analysis and in that of Rudd et al. (2008) could lie in the different efficiency of the feedback included in the simulations. In our case we include a rather efficient SN feedback, that could mitigate the effects of adiabatic contraction. Stanek et al. (2009) compared results for a non-radiative simulation and for a pre-heated radiative simulations. They found that at $\Delta = 500$ the latter predicts a HMF which is lower than the former. The reason for this

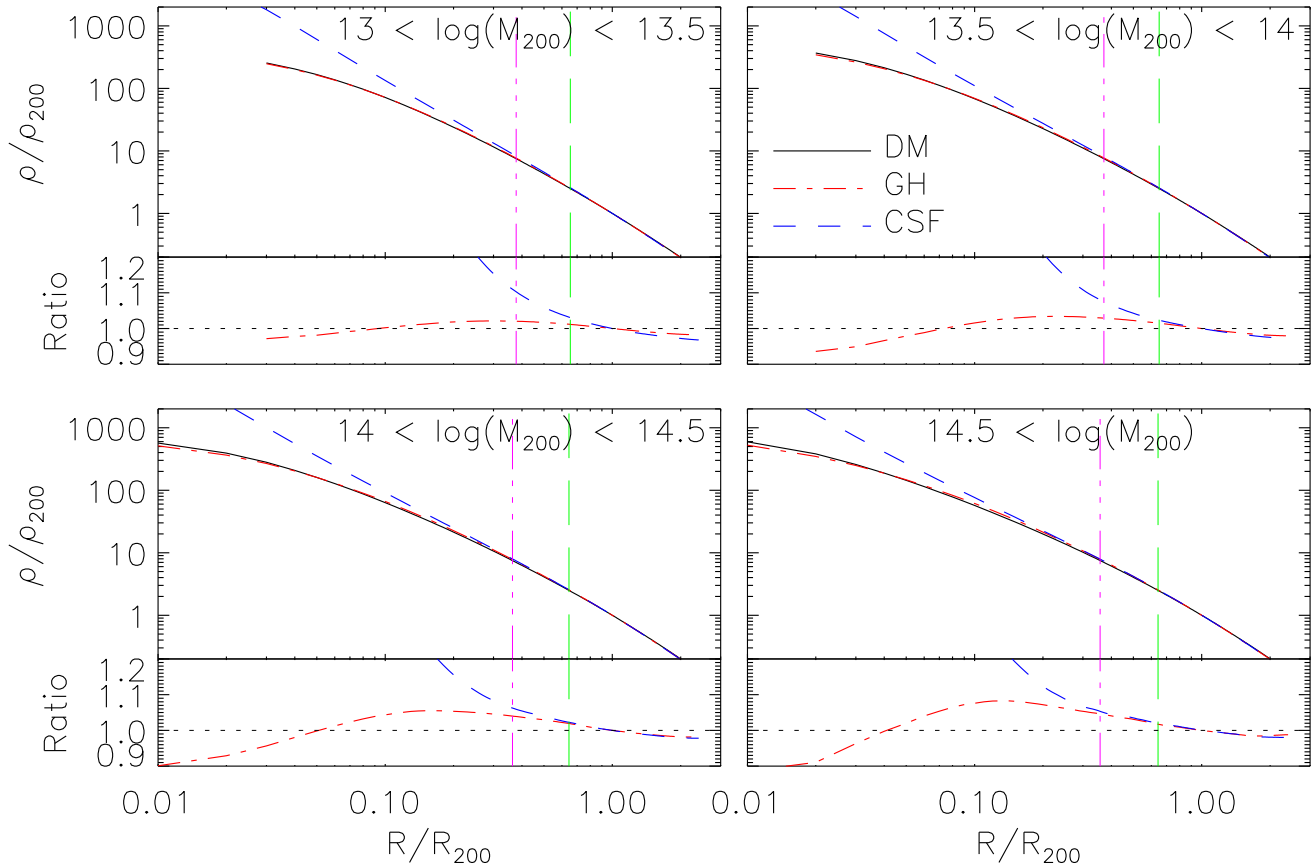


Figure 4. Mean radial profiles of the density within a given radius. Density is expressed in units of ρ_{200} , which is the mean density within R_{200} . In each panel, solid (black), dot-dashed (red) and dashed (blue) curves correspond to the DM, GH and CSF runs, respectively. The two vertical lines mark the mean value of R_{1500} and R_{500} for the DM simulation (purple triple-dot-dashed and green long-dashed lines, respectively). The four panels correspond to four different mass ranges over which the mean profiles are computed, as indicated in the labels.

is that the fairly strong pre-heating introduced in their simulation at $z = 4$ devoid halos by a substantial amount of gas, which is later prevented to re-accelerate in the forming larger halos.

Tinker et al. (2008) investigated the redshift evolution of the mass function computed at different values of Δ_c based on simulations including only dark matter. They found that the abundance of halos at a given $\log \sigma^{-1}$ monotonically decreases with increasing z in the interval $[0, 2.5]$, where σ is r.m.s. variance of the linear density field smoothed on a given mass scale. In the following we will discuss the impact that baryons in the GH and CSF simulations have on the evolution of the HMF.

We show in Figure 6 the evolution of the HMF at three different redshifts, $z = 0, 0.6$ and 1 , for $\Delta_c = 500$. Similarly to Fig. 5 we also show in the bottom panel the ratio between the HMF from each of the two hydrodynamical simulations and that of the DM simulation. In general, we find that the effect of baryons on the MF is to good approximation independent of mass at all redshifts for $\Delta_c = 500$. As for the non-radiative GH simulation, the increase of the HMF with respect to the DM case is always very small out to $z = 1$, and $\lesssim 8$ per cent. A more significant effect is instead found for the radiative CSF simulation. In this case the HMF

| Redshift | GH | | CSF | |
|-----------|------------------|------------------|------------------|------------------|
| | $\Delta_c = 500$ | $\Delta_c = 200$ | $\Delta_c = 500$ | $\Delta_c = 200$ |
| $z = 0.0$ | 1.037 | 1.012 | 1.049 | 1.016 |
| $z = 0.6$ | 1.028 | 1.000 | 1.044 | 1.005 |
| $z = 1.0$ | 1.028 | 0.997 | 1.040 | 0.999 |

Table 1. Mean values of the ratio between halo masses in the hydrodynamical and in DM simulations, at different redshifts and Δ_c values, for both the non-radiative (GH) and radiative (CSF) simulations. Such values have been computed by including only halos with $\log(M_{\Delta_c}/h^{-1} M_\odot) \geq 13.5$.

increases by a larger amount at progressively higher redshift, reaching the $\simeq 10$ per cent level at $z = 1$. This result agrees with the expectation that a more efficient cooling takes place at higher redshift, which induces a stronger effect on halo masses.

Due to the complexity and partial knowledge of the baryonic process taking place in galaxy formation, accurately calibrating the HMF from hydrodynamical simulation may appear a challenging task. However, owing to the results show in Fig. 3, it turns out that variation of halo masses in both GH and CSF simulations, with respect to

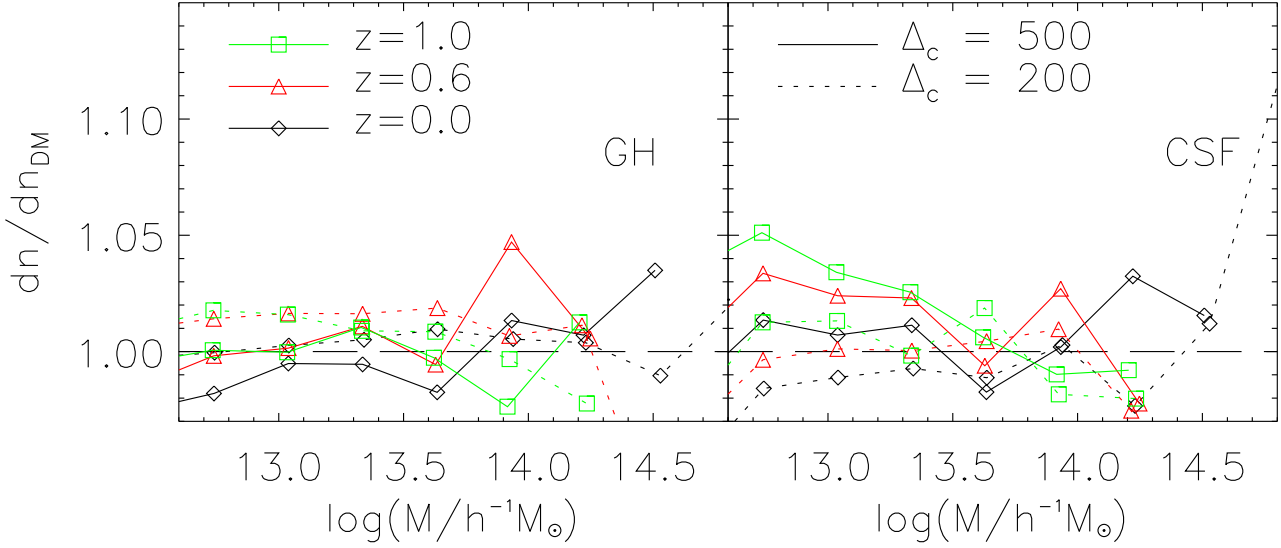


Figure 7. The number difference after halo mass calibration. Different colorful lines show the redshift, while the two line styles, solid and dotted represent $\Delta_c = 500, 200$, respectively. The left panel shows the corrected results for GH run, and the right is for CSF run.

the pure DM case, is to good approximation independent of halo mass, at least for $\log(M/h^{-1} M_\odot) \geq 13.5$ and $\Delta_c = 200$ and 500. Therefore, we can in principle attempt to account for the effect of baryons in the HMF by a simple shift of halo masses, at least within the mass range and for the Δ_c values for which is approximation is expected to hold. In Table 1 we report the average values of the mass ratio for halos identified in the hydrodynamical and in the DM simulations, for different Δ_c and redshift values. This values, which are computed as an average over all halos having mass $\log(M_{\Delta_c}/h^{-1} M_\odot) \geq 13.5$, are then used to rescale the HMF from the hydrodynamical simulation.

In Figure 7, we show the ratio between the number of halos of different mass found in the hydrodynamical and in the DM simulations, after applying the mass shifts reported in Table 1. A larger mass binning is used here, $\Delta \log M = 0.3$, to reduce fluctuations associate to sampling noise. From the left panel of Figure 7, the difference in the halo number is now consistent with zero, with fluctuations around this value of $\lesssim 3$ percent for $\Delta_c = 500$. This result holds independently of mass and redshift, at least for halos with $\log(M_{\Delta_c}/h^{-1} M_\odot) \geq 13.5$. As expected, the correction is less effective for smaller masses, owing to the larger mass difference induced by baryonic effects in smaller halos. Clearly, the correction is less pronounced at $\Delta_c = 200$, owing to the smaller impact of baryons at this overdensity. However, also in this case, correcting the HMF according to a unique mass shift further reduces the difference between hydrodynamical and DM simulations at the 1–2 per cent level. The number difference for CSF run at $\Delta_c = 500$ is also suppressed to unity for all halos with $\log(M/h^{-1} M_\odot) \geq 13.5$.

In conclusion, the results obtained from our analysis indicates that the relative variation of halo masses due to baryon effects are always within 5 per cent, for both non-radiative and radiative simulations, also almost independent of redshift. This result holds for masses computed at overdensity $\Delta_c = 200$ and 500, and for halos having mass at least comparable to that of a galaxy group. Correcting the

mass function with a constant mass shift in this mass range largely accounts for the differences between hydrodynamical and DM simulations.

4 DISCUSSION AND CONCLUSION

In this paper we presented an analysis of the effect of baryons on the calibration of the halo mass function (HMF). To this purpose, we carried out one DM-only simulation (DM) and two hydrodynamical simulations, a non-radiative one including only the effect of gravitational gas heating (GH) and a radiative one including also the effect of star formation and SN feedback in the form of galactic ejecta. The three simulations, which are all based on the Tree-PM/SPH GADGET-3 code (Springel 2005a), started from exactly the same initial conditions and followed the evolution of 2×10^4 particles within a box having a comoving size of $410 h^{-1}$ Mpc. Halos have been identified using a spherical overdensity (SO) algorithm, and results have been presented at three redshifts, $z = 0, 0.6$ and 1. Halo masses have been computed at different overdensities (with respect to the critical one), $\Delta_c = 200, 500$ and 1500. The main results of our analysis can be summarized as follows.

1. The fractional difference between halo masses in the hydrodynamical and in the DM simulations is found to be almost constant, at least for halos more massive than $\log(M_{\Delta_c}/h^{-1} M_\odot) \geq 13.5$. In this range, the mass increase in the hydrodynamical simulations is of about 4–5 per cent at $\Delta_c = 500$ and 1–2 per cent at $\Delta_c = 200$. Quite interestingly, these differences are nearly the same for the GH and the CSF simulations (see Fig.3 and Table 1). Such relative mass variations can not be considered any more as constant at higher overdensity, $\Delta_c = 1500$, and smaller masses. In these cases, mass difference markedly increases for smaller halos in the CSF simulation, while it decreases in the non-radiative GH simulation.
2. These variations of halo masses induce corresponding

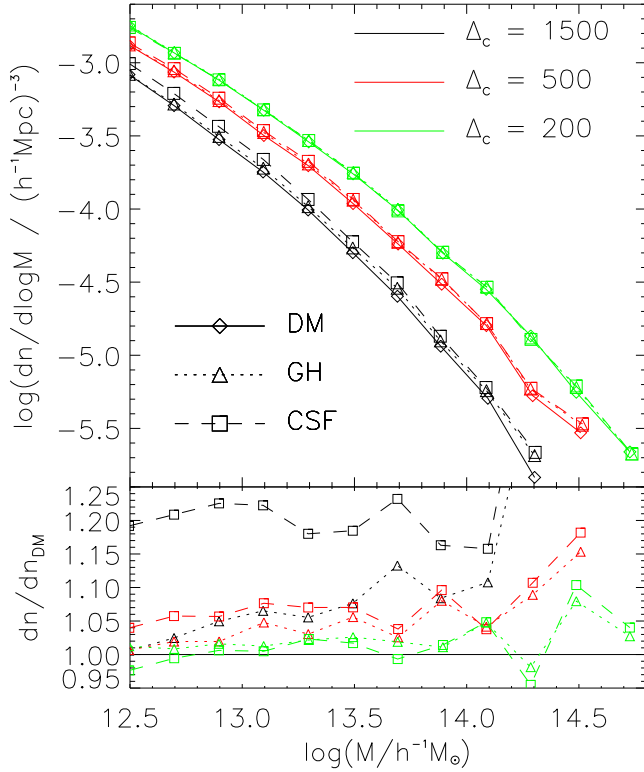


Figure 5. The halo mass function for our simulations, with masses computed at different overdensities Δ_c . Results for the DM simulations are shown with dotted curves, while results for the GH and CSF hydrodynamical simulations are shown with the dashed and dot-dashed curves, respectively. Upper to lower curves correspond to result for $\Delta_c = 200$, 500 and 1500 (green, red and black curves, respectively). The lower panel shows the ratio between the number of halos found in each mass bin for each of the two hydrodynamical simulation and the DM simulation. We apply a linear interpolation of the mass functions to compute the difference in the halo number exactly for the same mass values.

variations of the HMF (see Fig. 5). At $z = 0$, the HMFs for GH and CSF simulations are close to the DM one, with differences of $\lesssim 3$ per cent at $\Delta_c = 200$, in line with the small correction in halo masses. Such a difference increases to $\simeq 7$ per cent at $\Delta_c = 500$ and reaches ~ 10 –20 per cent at $\Delta_c = 1500$. At the latter overdensity, the increase in the HMF for the CSF run is larger by about a factor 2 with respect to the GH run. This result is in line with the expectation that baryonic processes have a stronger impact in the central halo regions. At higher redshift, differences with respect to the DM HMF tend to increase, especially for $\Delta_c = 1500$ (see 6) and for the CSF case. Again, this result agrees with the increase of cooling efficiency within halos at higher redshift.

3. Based on the above results, we showed that assuming a constant mass variation to rescale the HMF from the hydrodynamic simulations reduces the difference with respect to the DM case. We apply a uniform mass shift, calibrated for halo masses $\log(M h^{-1} \text{M}_\odot) \geq 13.5$ for $\Delta_c = 200$ and 500. We verified that the difference between hydrodynamical and DM HMFs becomes negligible, with fluctuations around null

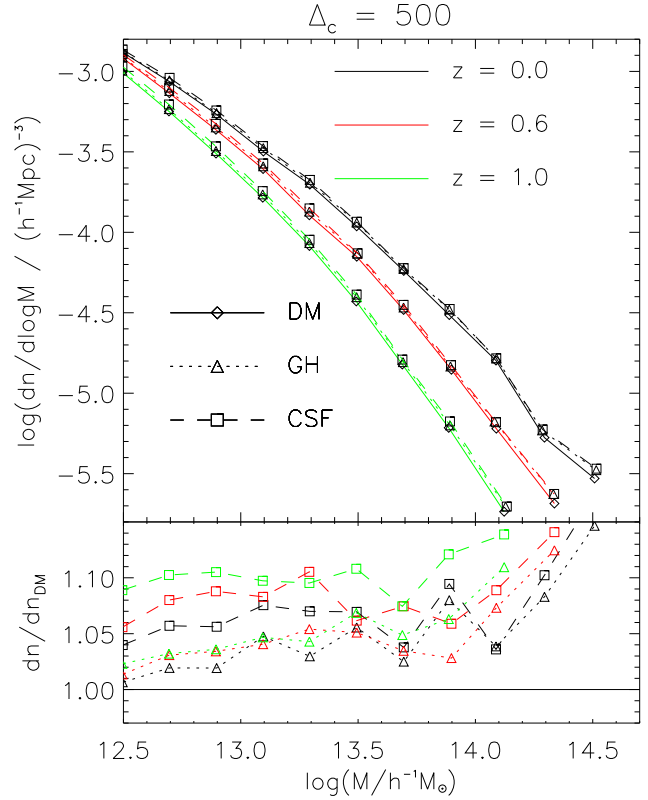


Figure 6. The redshift evolution of the halo mass function for our simulations, with masses computed overdensity $\Delta_c = 500$. Results for the DM simulations are shown with dotted curves, while results for the GH and CSF hydrodynamical simulations are shown with the dashed and dot-dashed curves, respectively. Upper to lower curves correspond to result for $z = 0.00$, 0.58 and 1.00 (black, red and green curves, respectively). The lower panel shows the ratio between the number of halos found in each mass bin for each of the two hydrodynamical simulation and the DM simulation.

of $\lesssim 3$ per cent at $\Delta_c = 500$. Even though mass variations are smaller at $\Delta_c = 200$, we still find that a uniform mass rescaling gives a small but sizable reduction of the HMF difference also at this overdensity.

The future generation of large surveys of galaxy clusters, from X-ray, optical and Sunyaev-Zeldovich observations, could provide stringent constraints of cosmological parameters through the study of the evolution of the mass function. However, a necessary condition to fully exploit the cosmological information content of such surveys is that the theoretical mass function needs to be calibrated to a precision better than 10 per cent (e.g. Wu et al. 2010). In this respect, the results of our analysis have interesting implications to gauge the uncertainty in the mass function calibration associated to the uncertain baryon physics.

First of all, the HMF turns out to be less prone to such effects if computed at $\Delta_c = 500$, while they become more important and likely difficult to model in detail at higher overdensities. Furthermore, adopting a constant mass shift provides a rather accurate correction to the HMF calibrated from DM simulations, at least for halos having size or galaxy groups or larger. This result holds for both the non-

radiative (GH) and the radiative (CSF) simulations, which have rather similar mass corrections at $\Delta_c = 500$. Since the CSF run only include SN feedback, but no AGN feedback, clusters in this simulations still suffers for overcooling. Therefore, the GH and CSF simulations should in principle bracket the case in which the correct amount of baryons cools within DM halos. However, we note that Stanek et al. (2009) found a slight decrease, rather than an increase of the HMF in simulations including an impulsive pre-heating. Since a phenomenological pre-heating only provides an approximate description of the astrophysical mechanisms regulating star formation, it would be interesting to repeat our analysis also in the presence of a mechanism for AGN feedback that regulates cooling in groups and clusters to the observed level (e.g., Puchwein et al. 2008; Fabjan et al. 2010; McCarthy et al. 2010).

Another direction in which our analysis should be improved concerns the size of simulation box, so as to better sample the population of massive halos. Although our results indicate that a mass-independent mass shift should be applied to account for baryonic effects, one may wonder whether this prescription can be extrapolated to the most massive halos, whose population is mostly sensitive to choice of the cosmological model. Future development in supercomputing capabilities will soon open the possibility to carry out hydrodynamical simulations which will cover dynamic ranges comparable to those accessible by the N-body simulations currently used to calibrate the halo mass function.

ACKNOWLEDGEMENTS

The authors would like to thank anonymous referee for useful suggestions and Pierluigi Monaco, Susana Planelles for valuable discussions. Simulations have been carried out in CINECA (Bologna), with CPU time allocated through IS-CRA. Weiguang Cui acknowledges a fellowship from the European Commission's Framework Programme 7, through the Marie Curie Initial Training Network CosmoComp (PITN-GA-2009-238356). This work is partially supported by the PRIN-INAF-2009 Grant "Toward an Italian network for computational cosmology" and by the PD51-INFN grant.

REFERENCES

- Allen S. W., Evrard A. E., Mantz A. B., 2011, ArXiv e-prints
- Baugh C. M., 2006, Reports on Progress in Physics, 69, 3101
- Bhattacharya S., Heitmann K., White M., Lukić Z., Wagner C., Habib S., 2011, ApJ, 732, 122
- Borgani S., Murante G., Springel V., Diaferio A., Dolag K., Moscardini L., Tormen G., Tornatore L., Tozzi P., 2004, MNRAS, 348, 1078
- Casarini L., Macciò A. V., Bonometto S. A., Stinson G. S., 2011, MNRAS, 412, 911
- Cohn J. D., White M., 2008, MNRAS, 385, 2025
- Crocce M., Fosalba P., Castander F. J., Gaztañaga E., 2010, MNRAS, 403, 1353
- Davis M., Efstathiou G., Frenk C. S., White S. D. M., 1985, ApJ, 292, 371
- Duffy A. R., Schaye J., Kay S. T., Dalla Vecchia C., Battye R. A., Booth C. M., 2010, MNRAS, 405, 2161
- Fabjan D., Borgani S., Tornatore L., Saro A., Murante G., Dolag K., 2010, MNRAS, 401, 1670
- Gnedin O. Y., Kravtsov A. V., Klypin A. A., Nagai D., 2004, ApJ, 616, 16
- Gonzalez A. H., Zaritsky D., Zabludoff A. I., 2007, ApJ, 666, 147
- Jenkins A., Frenk C. S., White S. D. M., Colberg J. M., Cole S., Evrard A. E., Couchman H. M. P., Yoshida N., 2001, MNRAS, 321, 372
- Jing Y. P., Zhang P., Lin W. P., Gao L., Springel V., 2006, ApJL, 640, L119
- Lacey C., Cole S., 1994, MNRAS, 271, 676
- Lagana T. F., Zhang Y.-Y., Reiprich T. H., Schneider P., 2011, ArXiv e-prints
- Lin W. P., Jing Y. P., Mao S., Gao L., McCarthy I. G., 2006, ApJ, 651, 636
- Lukić Z., Heitmann K., Habib S., Bashinsky S., Ricker P. M., 2007, ApJ, 671, 1160
- McCarthy I. G., Schaye J., Ponman T. J., Bower R. G., Booth C. M., Dalla Vecchia C., Crain R. A., Springel V., Theuns T., Wiersma R. P. C., 2010, MNRAS, 406, 822
- More S., Kravtsov A., Dalal N., Gottlöber S., 2011, ArXiv e-prints
- Pedrosa S., Tissera P. B., Scannapieco C., 2009, MNRAS, 395, L57
- Press W. H., Schechter P., 1974, ApJ, 187, 425
- Puchwein E., Sijacki D., Springel V., 2008, ApJL, 687, L53
- Rasia E., Tormen G., Moscardini L., 2004, MNRAS, 351, 237
- Reed D., Gardner J., Quinn T., Stadel J., Fardal M., Lake G., Governato F., 2003, MNRAS, 346, 565
- Reed D. S., Bower R., Frenk C. S., Jenkins A., Theuns T., 2007, MNRAS, 374, 2
- Rudd D. H., Zentner A. R., Kravtsov A. V., 2008, ApJ, 672, 19
- Sheth R. K., Tormen G., 1999, MNRAS, 308, 119
- Springel V., 2005a, MNRAS, 364, 1105
- Springel V., 2005b, MNRAS, 364, 1105
- Springel V., Hernquist L., 2003, MNRAS, 339, 289
- Springel V., White S. D. M., Jenkins A., Frenk C. S., Yoshida N., Gao L., Navarro J., Thacker R., Croton D., Helly J., Peacock J. A., Cole S., Thomas P., Couchman H., Evrard A., Colberg J., Pearce F., 2005, Nature, 435, 629
- Stanek R., Rudd D., Evrard A. E., 2009, MNRAS, 394, L11
- Sutherland R. S., Dopita M. A., 1993, ApJS, 88, 253
- Tinker J., Kravtsov A. V., Klypin A., Abazajian K., Warren M., Yepes G., Gottlöber S., Holz D. E., 2008, ApJ, 688, 709
- Tissera P. B., White S. D. M., Pedrosa S., Scannapieco C., 2010, MNRAS, 406, 922
- Tornatore L., Borgani S., Dolag K., Matteucci F., 2007, MNRAS, 382, 1050
- van Daalen M. P., Schaye J., Booth C. M., Dalla Vecchia C., 2011, MNRAS, pp 1079–+
- Warren M. S., Abazajian K., Holz D. E., Teodoro L., 2006, ApJ, 646, 881

White M., 2001, A&A, 367, 27

White M., 2002, ApJS, 143, 241

Wu H.-Y., Zentner A. R., Wechsler R. H., 2010, ApJ, 713,
856

Zentner A. R., Rudd D. H., Hu W., 2008, Phys Rev D, 77,
043507

This paper has been typeset from a \TeX / \LaTeX file prepared
by the author.